



Gold-decorated sulfur-doped carbon nanotubes as electrocatalyst in hydrogen evolution reaction

Hossein Tavakol¹ · Mohammad Zhiani¹ · Fereshteh Shareifyan-ghahfarokhi¹

Received: 10 December 2019 / Accepted: 3 April 2020 / Published online: 2 May 2020
© Springer Nature Switzerland AG 2020

Abstract

In the present work, sulfur-doped carbon nanotubes (SCNTs) have been prepared using chemical vapor deposition method and various cobalt-containing catalysts. In this line, simple and silica-supported cobalt nanoparticles (Co and Co/SiO₂) and 5 cobalt spinels (MCo₂O₄, M = Ni, Cu, Mn, Fe, Cr, and Mg) were used as the growth catalysts and four different temperatures (600, 650, 700, and 750 °C) were used to obtain the optimized condition for the preparation of SCNTs. Among the employed catalysts, Co/SiO₂ at 600 °C showed the higher abilities for the preparation of desired SCNTs. All products were characterized using FESEM, EDS, XRD, Raman, static contact angle, TGA, and DTA analyzes. The electrochemical behaviors of the two best products (SCNTs-Co/SiO₂ and SCNTs-Co) in hydrogen evolution reaction (HER) were examined, which confirmed the higher ability of SCNTs-Co/SiO₂. This best product was decorated with 2, 5, and 10% of gold nanoparticles to examine the effect of gold decoration of the properties and electrochemical abilities of the product. All decorated products exposure the higher electrochemical potencies versus the simple SCNTs and among the decorated products, 10% Au-SCNT was the most appropriate product for this purpose with small differences with the other ones.

Keywords CNT · Doping · Decoration · Gold · Surface · Electrocatalyst

Introduction

Carbon nanotubes (CNTs) are nanostructured cylindrical allotrope of carbon, which could be presented by rolling a single or multiple sheet of graphene. After the first discovery of CNTs, their structures, synthesis, and applications have been investigated by various scientists because of their enormous potentials as advanced materials [1–3]. Due to their special one-dimensional structure, they could have metallic or semi-conducting electrical conductivity [4]. These materials have been used in several environmental applications, separation filters, membranes, and water treatment [5–9]. They have specialized properties such as high electrical and thermal conductivity, appropriate elasticity, and high electromagnetic absorption [10–12]. Many electronic devices, especially Li-ion batteries, supercapacitors and solar cells have been made from

these materials [13–20]. The other applications of these materials are in drug delivery, sensors, actuators, detectors, fluorescence imaging, nanoelectronics, and wearable electronics [21–24].

Among different possible synthetic methods for preparation of CNTs (arc discharge, laser ablation, plasma, and solvothermal), chemical vapor deposition (CVD) has more benefits such as low price and possibility of large-scale preparation [25]. Therefore, several investigations have been reported for the CVD synthesis of CNTs [26]. However, the basic properties of CNTs have not been convincing for many researchers and they looked for different methods to change and enhance their electronic, mechanical, adsorption, and other properties by adjusting their structures [27, 28]. For this purpose, several methodologies such as physical correction, decoration, chemical functionalization, and doping have been developed [29, 30]. The doping of CNTs has attracted great attentions because of its prominent effects on the electrical and sensor properties of CNTs [31]. In this line, a several theoretical and experimental studies related to the doping of CNTs have been published [32–34]. However, the doping of row-3 elements (such as sulfur, phosphorus, and silicon) are less studied because of their large atomic radius and harder

✉ Hossein Tavakol
h_tavakol@iut.ac.ir

¹ Department of Chemistry, Isfahan University of Technology, Isfahan 84156-83111, Iran

conditions for their preparation. Therefore, since several years ago, this group has been focused on the synthesis and application of doped CNTs with row-3 elements [35, 36]. To develop our knowledge and potencies for the synthesis of doped CNTs, presenting new catalysts with appropriate properties and higher potencies should be investigated. During the recent years, several works has been reported on the use of different catalysts for the preparation of simple and doped CNTs [37]. However, presenting new catalysts for the synthesis of doped CNTs with row-3 elements are limited to a few numbers. Therefore, it has been focused on the effective preparation of sulfur-doped CNT (SCNT) with the desired properties using new catalyst (cobalt-based nanocatalysts) and examine its ability in a potential and important application, electrocatalyst in hydrogen evolution reaction (HER).

Development of effective technologies for clean and sustainable hydrogen energy has been drawn increasing attention in the past few years, as hydrogen is hailed as a promising energy source to reduce our dependence on fossil fuels and benefit the environment by reducing the emissions of greenhouse and other toxic gases. Toward this end, an effective and promising approach is based on the electrolysis of water for hydrogen production. In this line, gold-containing materials showed desirable abilities in catalyzing different processes [38–41]. Electrocatalytic HER, preferably driven by solar energy, is a highly attractive methodology for meeting these requirements [42]. In electrocatalysis, carbon nanostructures have gathered important interests due to their obvious advantage in acting as metal catalyst supports for boosting the energy-relevant important electrochemical reactions such as HER. However, by modifying the structure of CNTs with the help of another elements such as sulfur and nitrogen, the product can be used in the reaction of hydrogen interaction with proper returns [43]. Therefore, it was focused to prepare the modified CNT (with both doping and decoration methods) and use the product for this purpose in the present work.

Experimental

Materials

Distilled water was used as a solvent in all experiments. Cobalt chloride (99.0%, Merck), aqueous hydrazine (80.0%, Merck), ethanol (96% purity, Bidestan Co, Qazvin, Iran), HF (40%, Merck), silica (99.99% purity, 15 m²/g and grains of 325 mesh), and NaOH (industrial grade) were bought and used without purification. Acetylene (99.99% purity) and argon (99.99% purity) gases were bought from Tebgas Co (Isfahan, Iran). Sulfur powder (industrial grade) was obtained from Pars chemical Co (Isfahan, Iran).

Instruments

The growth step was done using a dual electric tube furnace (designed by Nano sat Co, Semnan, Iran; www.nanosatco.com). This instrument is consisted of a quartz tube with 100 cm length and 5 cm internal diameter. Field emission scanning electron microscopy (FESEM), X-ray energy-dispersive spectrometry (EDS), and elemental mapping analyses have been performed using Mira 3-XMU FE-SEM (Tescan Co, Brno, Czech Republic). Transmission electron microscopy (TEM) analysis was performed using EM208S TEM microscope (Philips Co, The Netherland). In addition, powder X-ray diffraction (XRD) spectrum was recorded by XPERT instrument (Philips Co, The Netherland) using Cu as a radiation source. Moreover, Raman spectra were obtained using Senterra (Bruker Co, USA). The thermogravimetric curve of the precipitate was taken using a TGA-STA BAHR 503 (Germany), heated from room temperature to 800 °C at a rate of 5 °C/min under inert atmosphere at a gas flow rate of 50 mL/min, and then cooled naturally. ICP analyses were performed using Perkin–Elmer optima 7300 spectrometer. The catalytic activity of the synthesized CNTs in the hydrogen production reaction has been measured in the SAMA500 electrolyzer system. This set contains three electrodes, Ag/AgCl as the reference electrode, platinum as working electrode, and a GCE-modified with the product. The static contact angle was recorded using the U1000 microscopy camera and analyzed by cooling-tech microscope software.

The preparation of catalysts

The Co(0) nanoparticles on silica support (briefly named as Co/SiO₂) and were prepared by employing some adjustment of the reported work [44]. In a 250-mL beaker, 0.9 g silica was dispersed in 100 mL of ethanol-deionized water mixture (30:70 v/v). Then, 0.1 g cobalt chloride was added while the mixture was stirring. The pH of the solution was retained in about 8 by the addition of NaOH 3.8 M (controlled with paper pH-meter). The suspension was stirred for 6 h at room temperature. The solvent was then evaporated at 80 °C and the obtained solid was dried for 16 h at 100 °C to obtain Co (OH)₂. Then, a 500-mL, 3-necked reaction flask, equipped reflux condenser was placed in oil bath on the heater-stirrer. The reaction was performed under argon atmosphere, and an internal thermocouple was used for the control of the reaction temperature. The prepared Co(OH)₂ was introduced in the reaction flask, filled with 120 mL of distilled water. The suspension was stirred for 40 min at room temperature, and then 40 mL of hydrazine solution (80% in water) and 15 g NaOH were added. The pH of the solution was kept between 10 and 12, and the reaction mixture was slowly heated from room temperature to 80 °C for 4 h (up to the observation of black

precipitate). The black suspension was maintained at this temperature for 60 min and cooled to room temperature. Then, it was separated from the solution using a supermagnet and washed with water until neutral pH was obtained. The filtrate was dried at 60 °C under vacuum. The resulting solid was stored under argon. The final catalyst was prepared by calcinations of the dried solid under argon atmosphere at 300 °C for 3 h and then at 400 °C for 1 h.

The synthesis of Co(0) nanoparticles (without support, briefly named as Co) was performed according to the above steps, except the use of silica. The synthesis of various cobalt spinels (MCo_2O_4 , $M = Ni, Cu, Mn, Fe, Cr, \text{ and } Mg$) have been performed exactly according to the reported study [45].

The growth and purification of SCNTs

First, in order to obtain the optimal initial conditions for the synthesis of simple and doped CNTs, different temperatures and flow rates of feed and carrier gases were examined. To prepare simple CNTs, 0.05 g of catalyst transferred to an alumina boat (1×3 cm) and completely spread over the boat area. The boat was placed in the second thermal area of the CVD chamber. During the whole process, argon gas was passed through the furnace as an inert gas at a rate of 100 mL/min. To obtain sulfur-doped CNTs, 1 g of orthorhombic sulfur powder was put into an alumina boat and placed in first thermal area. The first thermal region has not been heated before the second zone was reached to the desired temperature. Based on the previous experiments, four temperatures (600, 650, 700, and 750 °C) have been considered for the second zone during the growth step. At this stage, acetylene gas was fed into the furnace for 30 min at a rate of 100 mL/min and argon gas was arranged at 50 mL/min. In order to optimize the flow rate of the gases entering the device, argon with a flow of 100 mL/min and acetylene gas with a flow of 200 mL/min entered the device and it was determined that by increasing the flow of acetylene gas to the device, the amount of amorphous carbons will be increased. It should be noticed that in the synthesis of sulfur-doped nanotubes, acetylene gas first entered the apparatus and after 5 min to coat the surface of the cobalt catalyst, when the growth of the nanotubes began, the temperature of the first zone would reach 500 °C. This process is necessary to ensure that sulfur could not react with cobalt. Otherwise, sulfur will inactivate the catalyst by poisoning and the growth of the nanotubes will not be done. After the end of the process, the furnace was cooled to the room temperature. The products were first placed at HCl solution (37%) with stirring for 2 h and then, in concentrated HF solution for 48 h and then placed under ultrasound radiation for 3 h. Then, CNTs were isolated by centrifugation followed by washing with distilled water several times.

Synthesis of gold-decorated SCNTs

The synthetic procedure described here is an adaptation of rapid colloidal gold nanoparticles (GNPs) method developed by Martin et al. with substantial modification for synthesis of Au-decorated SCNTs [46]. First, 0.1 g of CNTs with 5 mL of distilled water was placed under ultrasonic waves. For different amounts of decorated GNPs on SCNTs, the desired gold salt ($HAuCl_3$) was dissolved in 40 μ L HCl (37%) in a volumetric flask and reaches its volume to 10 mL by the addition of distilled water. A reductive solution by dissolving 0.019 g $NaBH_4$ and 0.02 g NaOH in distilled water in a 10-mL volumetric flask. Typically, the Au-SCNTs with 2% of GNPs are prepared as follows. First, CNTs were placed on the stirrer, and 200 μ L of gold solution was added to the CNTs. Then, 60 μ L of reductive solution was added at once. Then, the suspension was placed on the stirrer for 15 min and placed in an oven at 80 °C overnight. The solution was removed by filtration, and the solid product was washed with distilled water three times and dried in electric oven (120 °C for 4 h).

The catalytic ability of SCNTs in HER

The electrocatalytic activity of SCNTs was investigated by a three-electrode electrochemical cyclic voltammetry. A saturated calomel electrode (SCE) is utilized as a reference electrode. A platinum electrode is used as a counter electrode. The sample-coated glassy carbon electrode (GCE, 0.0706 cm^2) is adopted as a working electrode. The sample ink is composed of 2 mg sample dispersed in absolute ethanol solution containing nafion (5%) and sonicated for 8 h. Subsequently, 1 μ L of sample ink was dropped on the GCE and dried at ambient condition. The electrocatalytic activities were investigated by linear scanning voltammetry (LSV) at the HER region in KOH solution (1 M). The stability of the catalyst was investigated using chronoamperometric analysis at the same conditions.

Results and discussion

The preparation and characterization of SCNTs

At the beginning of this study and after some elementary experiment for the optimization of the basic parameters of the growth step (like the flow rates of the carrier and reagent gases, the temperature program and the quantity of sulfur powder), 8 different cobalt-based catalysts have been used in the growth step to examine their abilities for the preparation of the desired product. For this purpose, simple Co(0) nanoparticles, silica-supported Co(0) nanoparticles, and 6 cobalt spinels (MCo_2O_4 , $M = Ni, Cu, Mn, Fe, Cr, \text{ and } Mg$) have been synthesized and used in the growth step using the previously

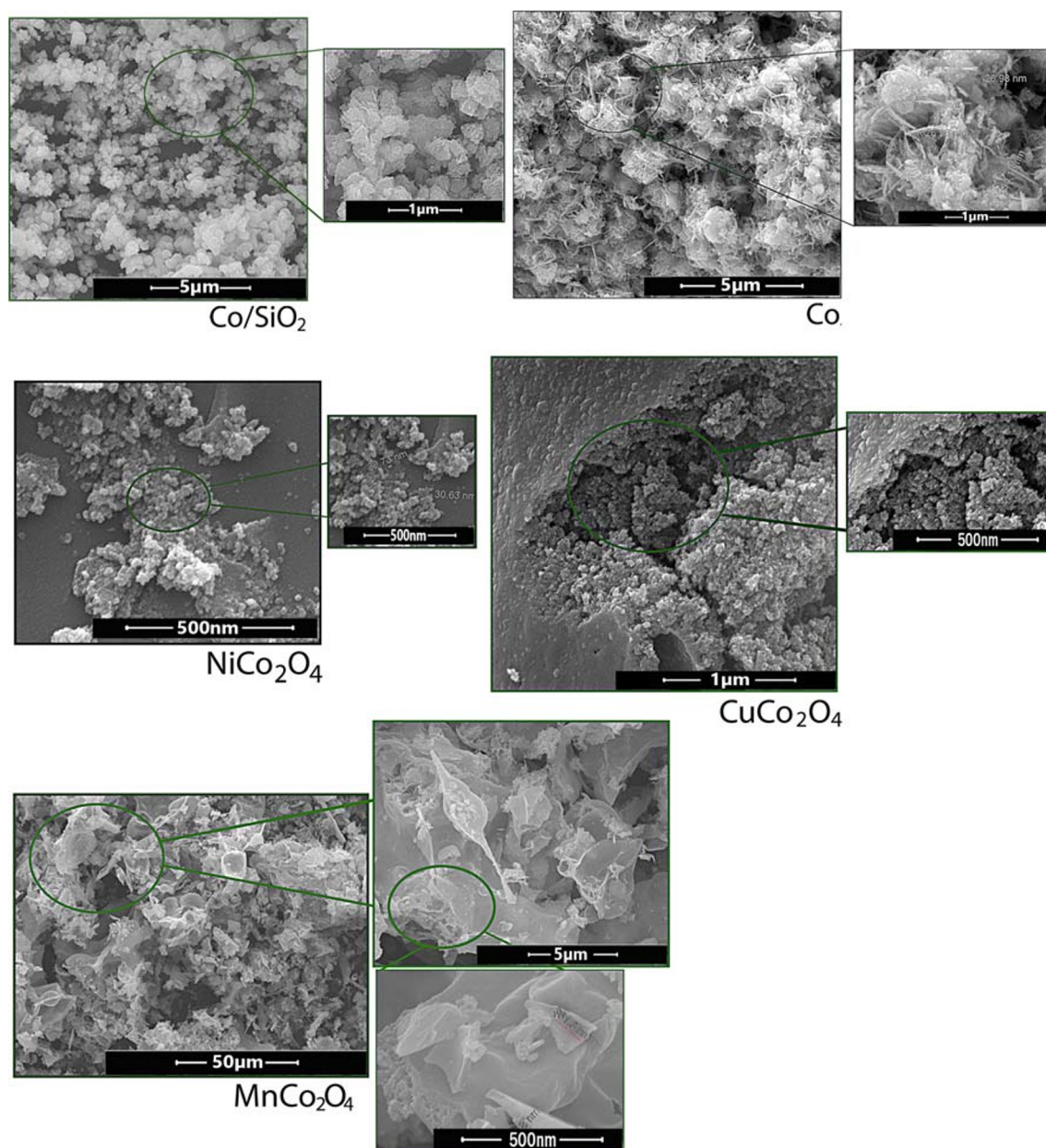


Fig. 1 The FESEM images of the prepared catalysts for the growth step

optimized conditions at 600 °C. Among these catalysts, the cobalt spinels of Fe, Cr, and Mg did not produce acceptable product (even by changing the growth conditions) and they have been ignored in this study, and the remaining 5 catalysts have been considered. The FESEM images of the prepared catalysts are shown in Fig. 1, and the EDS analyses and XRD patterns of them are depicted in Fig. 2. These catalysts have been employed to prepare the desired products (SCNTs) at the optimized conditions to obtain the best product for each of these catalysts.

According to the XRD pattern of Co/SiO₂, peaks observed in $2\theta = 42, 44, 48,$ and 62 degrees correspond to the cobalt (024), (015), (132), and (051) planes, respectively (reference code no.96-901-2585). There are other peaks at $2\theta = 31, 36, 38, 48,$ and 58 degrees, corresponding to the (022), (113), (222), (133), and (115) planes of SiCo₂O₄, based on the reports [47]. According to these peaks, cobalt nanoparticles existed in two crystalline forms. The decrease in the intensity of the three peaks measured at $2\theta = 42, 44,$ and 48 degrees for Co/SiO₂ versus Co corresponded to the reduction of the

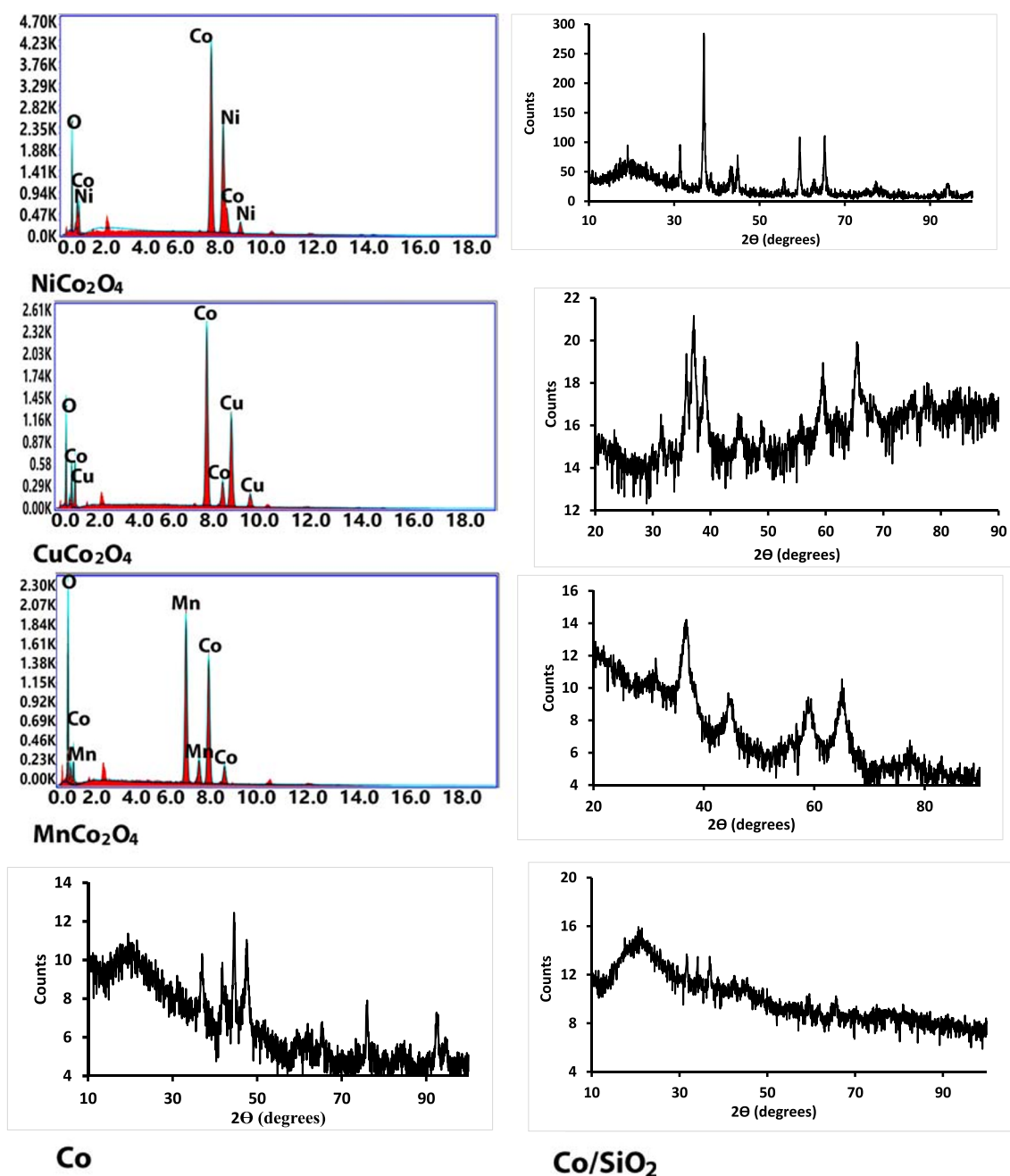


Fig. 2 The EDS spectra and XRD patterns of the cobalt catalysts

diameter of the metallic cobalt nanoparticles. For Co catalyst, the observed peaks are in $2\theta = 42, 44, 47.5, 62,$ and 75 degrees, corresponding to (010), (200), (011), (012), and (110) planes of hexagonal metallic cobalt with the reference code no. 0968-901-96 [48].

After the growth of carbon structures by different catalysts and the purification of the products, they have been analyzed using FESEM, EDS, and Raman analyses first. The results of FESEM analyses are shown in Fig. 3, and the related EDS and

Raman analyses are shown in Fig. 4 to compare the abilities of the catalysts for the preparation of the desired product. According to these images, the tube-like and cylindrical-shaped nanotubes were obtained only using Co and Co/SiO₂ catalysts and in other cases, the mixed structures were obtained. Based on the yields, the morphology of the product (from FESEM images), the purity of the product (from EDS analysis and experimental observations), and Raman spectra, using Co/SiO₂ as a catalyst, led to the most appropriate product,

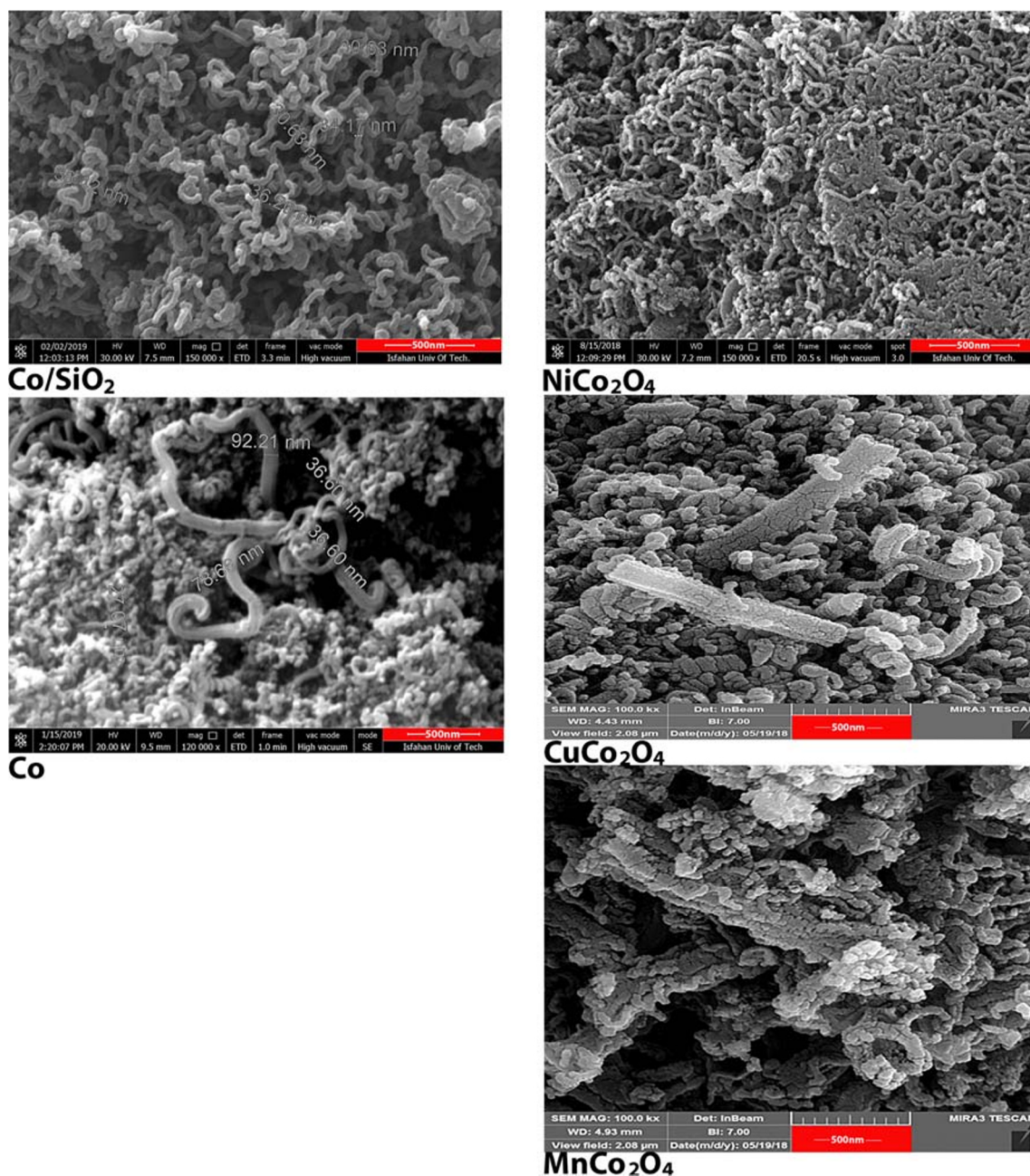


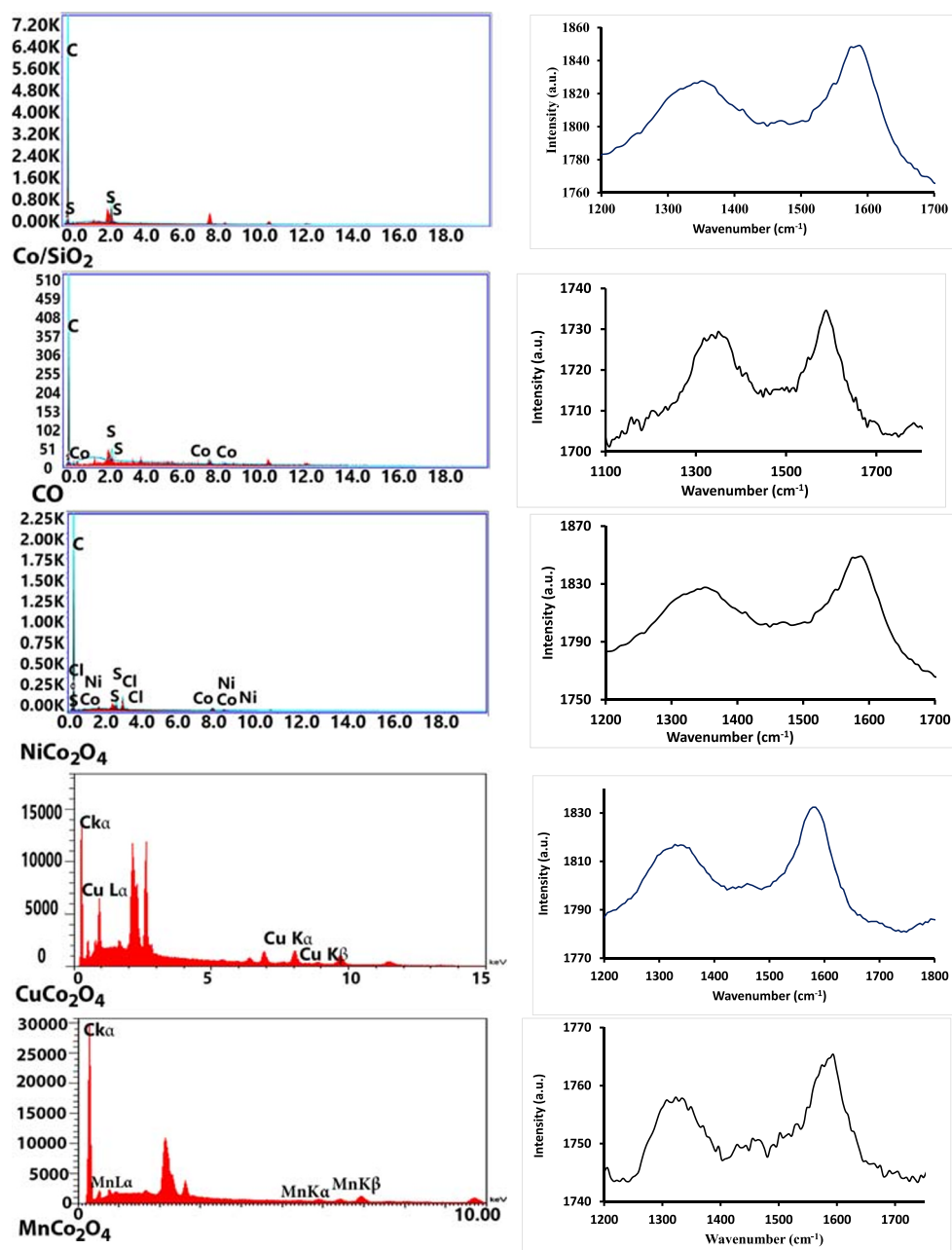
Fig. 3 The FESEM images of the prepared sulfur-doped carbon structures using different cobalt-containing catalysts

and this catalyst was selected as the best cobalt-containing catalyst for the preparation of SCNTs. The smaller diameter and more dispersity of the cobalt nanoparticles on silica surface, compared to nonsupported cobalt nanoparticles led to the production of more suitable products. Using this catalyst, the SCNTs have been prepared in the highest yields, the highest purity, the most uniform product, and the least ID/IG ratio (in Raman spectrum). The Co/SiO₂ catalyst and its product have been used in the next parts of this work, and the Co catalyst

was the second choice for this preparation while the other employed catalysts were not suitable for this preparation.

As the final optimization step, the effect of the growth temperature on the preparation of product using selected catalyst has been investigated. For this purpose, four different temperatures (600, 650, 700, and 750 °C) have been used in the growth step using the optimized conditions. The experiment at 600 °C was the repeating experiment to confirm the repeatability of the employed method.

Fig. 4 The EDS and Raman spectra of prepared materials using different cobalt-containing catalysts

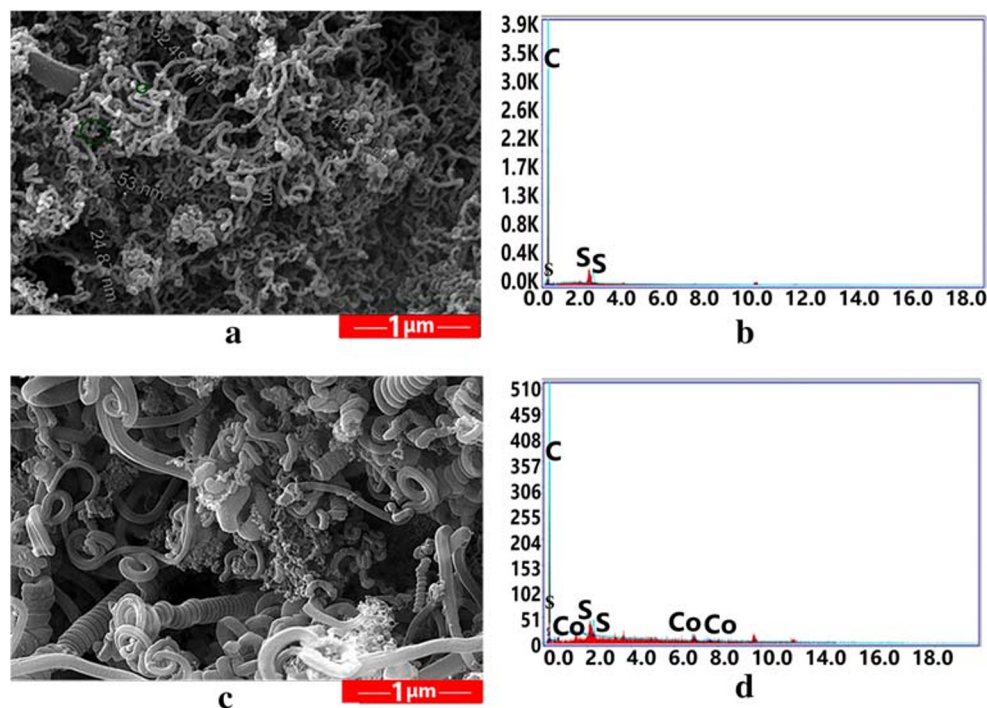


The FESEM images and EDS analyses of these experiments are shown in Fig. 5. Noticeably, using 700 and 750 °C as the growth temperature, the yield of the product was so low, they have deformed shapes, and most of the product has been wasted during the purification. Therefore, only the products prepared at 600 and 650 °C have been analyzed and shown in Fig. 5. According to the obtained analyses, the 650 °C product is less uniform, has larger sizes, and consisted of Co impurities. The structure of this product is spiral-shaped with various diameters, and it seems that the Co particles have

been strongly trapped in the product, which has not been eliminated during the purification step or any other reason. Therefore, based on this fault and because of the shape of the product, this product has not been considered as the main product of this study and 600 °C has been selected as the optimized temperature, and its product was chosen for the next investigations.

More details about the structure of selected product have been provided using TEM, TGA, DTA, and XRD analyses (Fig. 6), while its FESEM, EDS, and Raman analyses are

Fig. 5 The result of the optimization of the growth temperature. **a** FESEM images of the product at 600 °C (repeating test). **b** EDS of the product at 600 °C. **c** FESEM images of the product at 650 °C. **d** EDS of the product at 650 °C



shown in Figs. 3 and 4, previously. The TEM images confirm the structure of multiwalled SCNTs with diameters between 30 and 80 nm; their lengths are in micrometers and their wall thickness are between 5 and 20 nm. Like FESEM images, the prepared SCNTs have not arrayed orientations; instead, the tubes are mixed and twisted, showing spaghetti-type arrangement. As discussed before, the XRD analysis of the product shows noncrystalline graphite-like patterns, like the previous reports on the simple and doped CNTs. The TGA results show that there is no significant weight loss at temperature range 0–

200 °C. The weight loss before 200 °C is mostly because of the evaporation of solvent (water). It is noticeable that although the reaction was performed at 600 °C, we have used lots of water during the acid washing (for purification) of the product and water could be introduced into the structure during this step. The product has been dried after that, but this is possible to remain small portions of water in the structure and the whole weight loss before 200 °C is less than 0.5%. There is only less than 5% weight loss in the whole temperature area (0–800 °C). These values show the high temperature

Fig. 6 TEM images (top left), XRD patterns (top right), TGA (below left), and DTA (below right) of SCNTs

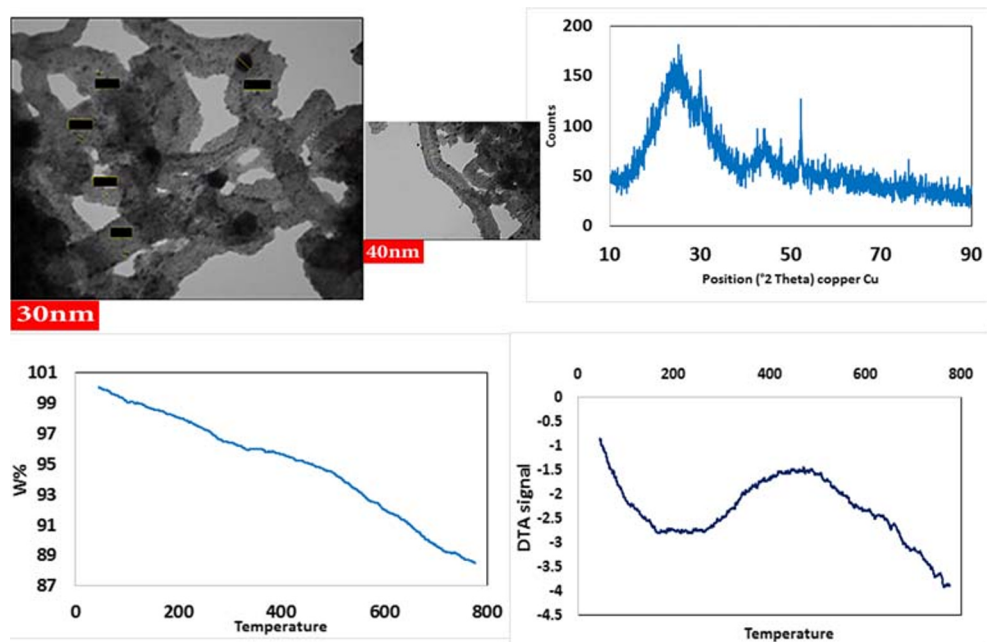
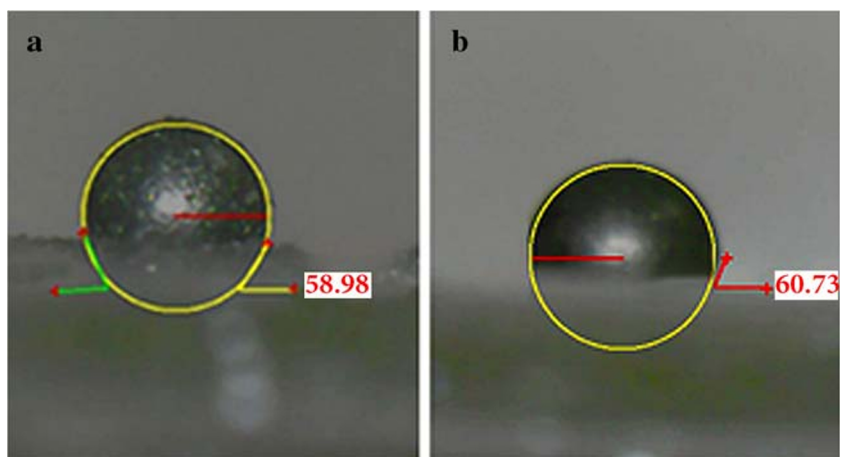


Fig. 7 The images of static contact angle test using water droplets on the surface of SCNTs. **a** Prepared using Co/SiO₂ catalyst. **b** Prepared using Co catalyst



resistance of the product, which is necessary property in the design of new advanced materials. There are three distinct weight loss area; the first one is about 1% in the range of 200 to 400 °C, the second slope is less than 2% in 400–500 °C, and the last one is more than 1% from 500 to 800 °C. The DTA diagram of the product is simple and consisted of two endothermic regions in 50–400 °C and 600–800 °C and one exothermic region in 400–600 °C. The endothermic peaks imply on the evaporation of adsorbed solvent and the fragmentation of the surface functionals and the exothermic peaks might be due to the adsorption of fragmented molecules or rearrangement of the structure.

The Raman spectrum of the product consists both D and G peaks as the major signals of the graphitic carbon materials. The G-band represents one-piece structure of the graphene-

hexagonal network and is due to the tensile vibration associated with the E_{2g} graphene network transmissions, and the D-band relates to the vibrational states caused by the presence of carbon with the sp³ hybrid and also indicates a defect or doped atom in the structure of the graphene network. The intensity of the G-band is a little stronger than the D-band tape in product and the ratio of the intensity of D to G (I_D/I_G ratio) is 0.98, which is in accordant with the previous studies related to the doped nanotubes. To examine the sulfur content of the product, the result of EDS analysis has been used. Based on these results, 3.7% of sulfur was observed for the multi-point EDS analysis. The real amount of the sulfur may be different because the EDS method only shows the surface content of each atom, but this value is a good estimate. The acceptable amount of surface sulfur content is necessary for the surface-gold

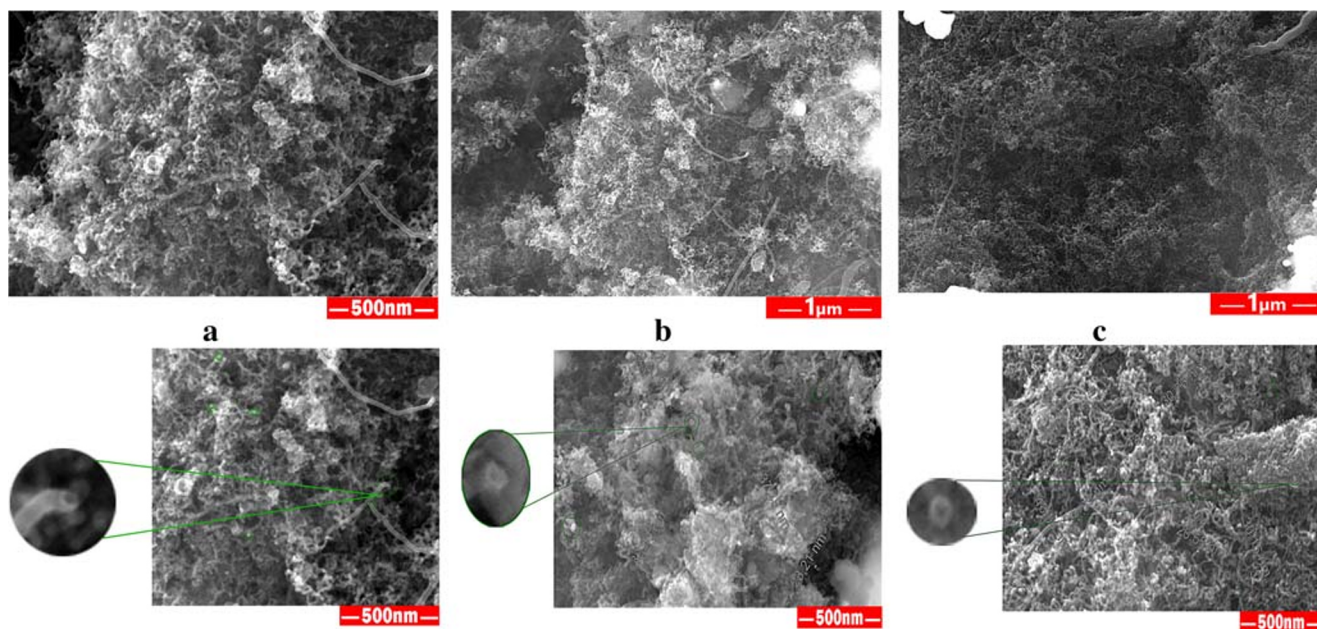


Fig. 8 FESEM images of Au-SCNTs with **a** 2% GNPs, **b** 5% GNPs, **c** 10% GNPs

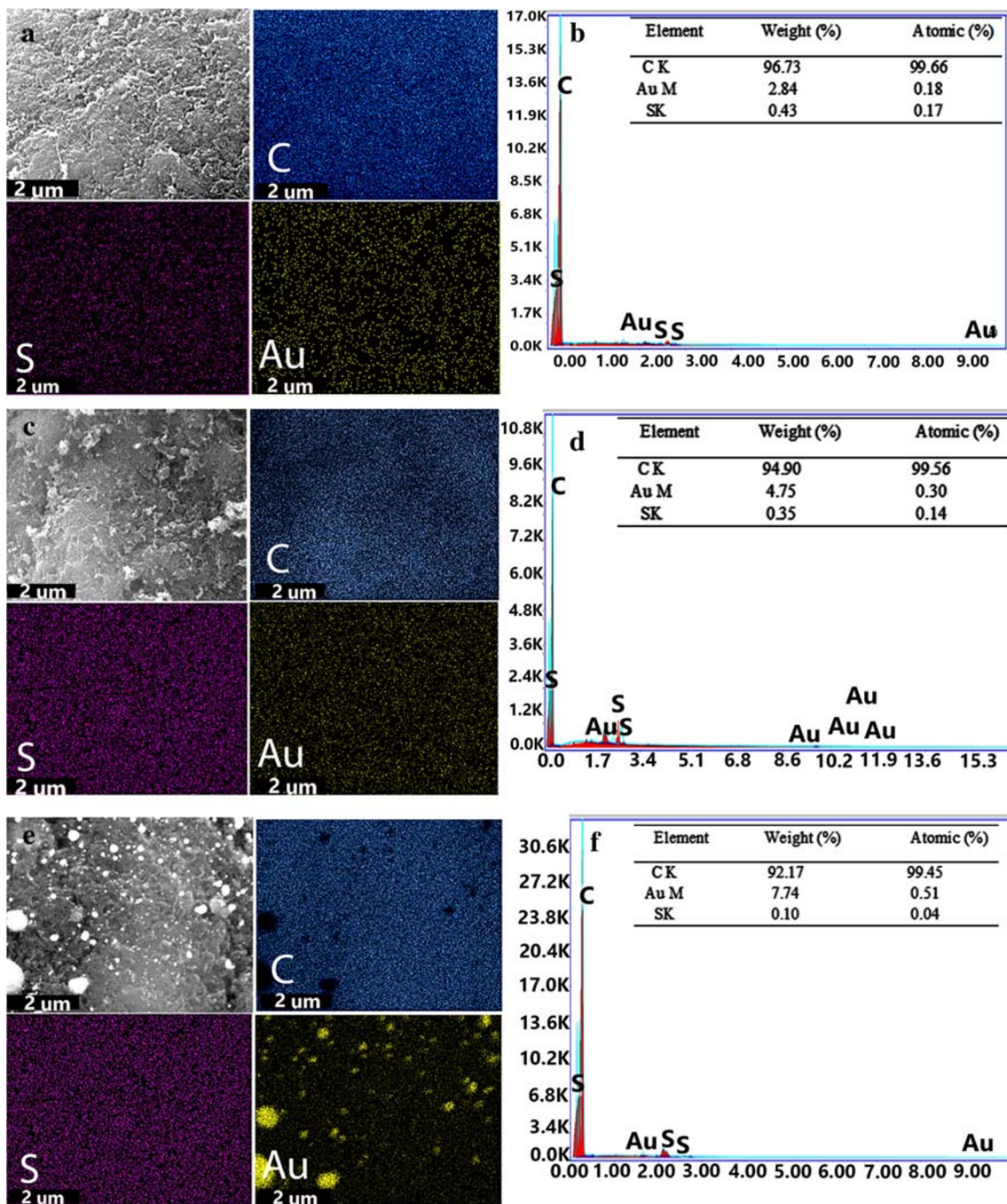


Fig. 9 a Elemental mapping images of 2%Au-SCNTs. b EDS of 2%Au-SCNTs. c Elemental mapping images of 5%Au-SCNTs. d EDS of 5% Au-SCNTs. e Elemental mapping images of 10%Au-SCNTs. f EDS of 10% Au-SCNTs

decoration of the product (next section) because of the strong sulfur-gold bond. Besides, by the increase of the amount of sulfur powder during the growth step, the sulfur content of the product has not been changed meaningfully. Moreover, it should be noticed that our products have been purified by two acid washing steps, which one of them was under ultrasound radiation. Therefore, all the pure, surface-adsorbed and undoped sulfur structures will be surely removed. The washing step is a standard way to remove all impurities (including

amorphous and undoped sulfur) other than the main structures, and the obtained S contents only show the doped sulfur atoms.

Table 1 The obtained weight percent of GNPs using various methods

Methods	10.0	5.0	2.0
Experimental	10.0	5.0	2.0
ICP	6.7	3.0	1.2
EDS	7.7	4.8	2.8

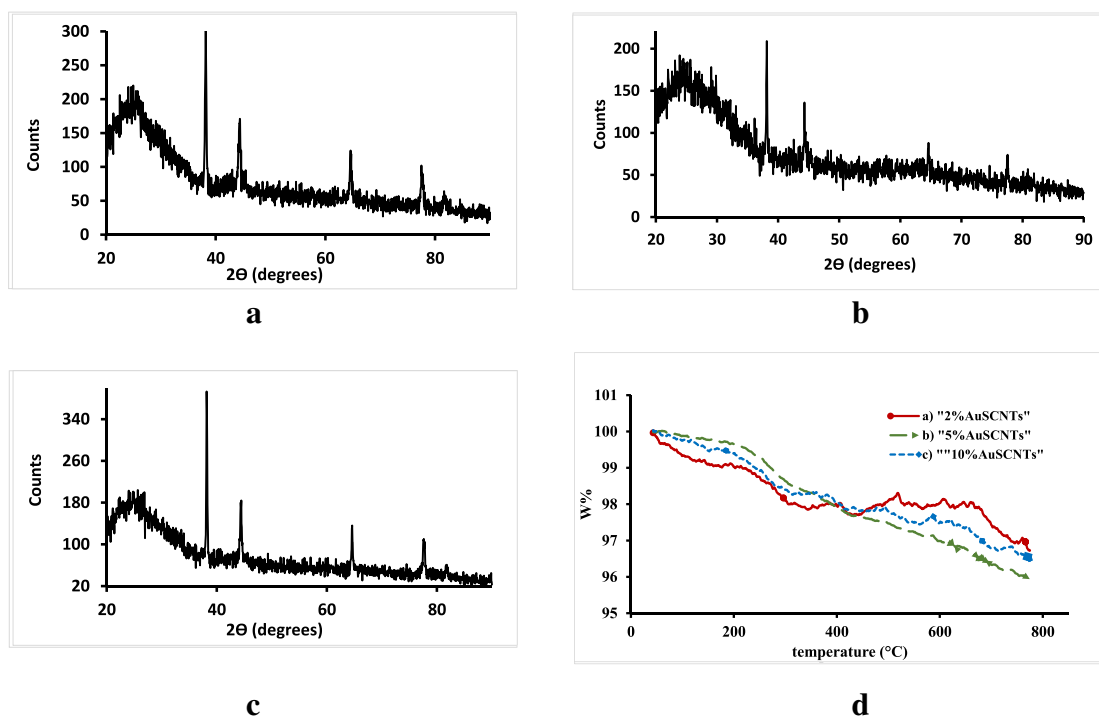


Fig. 10 The XRD pattern of **a** 2% Au-SCNTs, **b** 5% Au-SCNTs, and **c** 10% Au-SCNTs. **d** The TGA analyses of all decorated products

As the final characterization method, static contact angle test was performed using water droplets on the surface of prepared SCNTs using both Co/SiO₂ and Co catalysts, as shown in Fig. 7. This test is important since the most of prepared CNTs are strongly hydrophobic (contact angle larger than 80°) that limit their applications, especially their electrochemical applications (like the purpose of this work). However, using the presented doped nanostructures, the decrease of hydrophobic nature of the product was aimed. According to the obtained images from this test, the contact angles are 59.0° and 60.7°, respectively, for the product of Co/SiO₂ and Co catalysts, which confirm the successful decreasing of the hydrophobicity of the products. The difference between these products is so small, and both have moderate hydrophobic nature. The presence of doped sulfur and related surface oxygen atoms are responsible for the greater hydrophilicity of these products.

Table 2 Parameters extracted from the catalyst from LSV experiments in 1 M KOH solution

Sample	Onset (V)	−b (mV/dec)	J ₀ (mA/cm ²)
SCNTs-Co	−2.65	565	9.28
SCNTs-Co/SiO ₂)	−1.30	255	9.51
2% AuS-CNTs	−0.495	1228	15.01
5% AuS-CNTs	−0.498	865	15.05
10% AuS-CNTs	−0.496	670	15.01

Synthesis and characterization of gold-decorated SCNTs

At the second step of this work and after the successful synthesis of SCNTs, the surface of the product was decorated with different values (2, 5, and 10%) of GNPs to enhance their electrochemical and the other desired properties. The FESEM images of the synthesized products (named as 2%Au-SCNT, 5%Au-SCNT, and 10%Au-SCNT) are shown in Fig. 8, and their EDS analyses and elemental mapping images (for C, S, and Au) are depicted in Fig. 9. All these analyses have the general characteristics like the parent SCNTs as well as the new signals related to GNPs. The presence of small GNPs in FESEM images and the Au signal in EDS analyses are confirming evidences about the gold decoration of SCNTs. Moreover, elemental mapping images show the appropriate dispersion of GNPs on the surface of the product, without observable aggregation. Since the EDS analysis only show the surface content of the element, the amount of Au in these products have been analyzed using ICP method. The results of the ICP analyses were compared with EDS and experimental (the used content of gold in the procedure) values in Table 1. According to the obtained values, ICP values are less than the experimental values that show some of gold contents of the solution have not been sit on the product. However, the EDS values are higher than ICP values which show that most of GNPs were placed on the surface of the SCNTs, instead of trapping inside or between them.

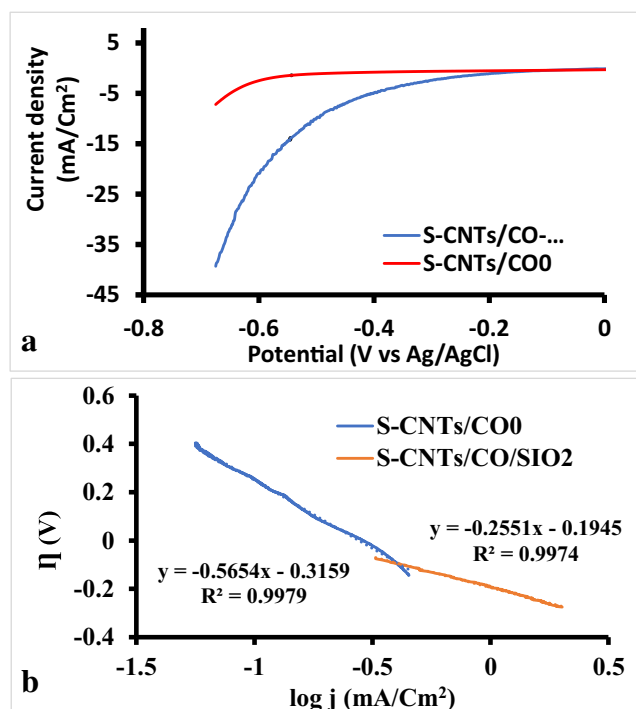


Fig. 11 a The LSV curves of the SCNTs in alkaline HER (in 1 M KOH). b The Tafel slopes chart for SCNTs as HER electrocatalyst

The decorated products were also analyzed using XRD method, and the results are depicted in Fig. 10. The XRD patterns consisted of both patterns of the SCNTs (like Fig. 6) and GNPs. The broad peaks at 26° and 44° correspond to the (002) and (100) graphitic plates. For GNPs, four sharp peaks at 38°, 44°, 65°, and 78° could be observed, related to the (111), (002), (220), and (311) planes of crystalline gold, respectively [49]. By the increase of GNP content, the relative sizes of these peaks have been increased.

Finally, these three decorated products were also analyzed using TGA analysis (Fig. 10, below right) to follow the variation of thermal stability of the SCNT after gold decoration. The thermal stabilities of all decorated products have been slightly increased because the total with losses for 2% Au-SCNT, 5% Au-SCNT, and 10% Au-SCNT are respectively 3.3, 4.0, and 3.4%, which all of them showed less weight loss than nondecorated SCNTs. In the thermal decomposition graph of these decorated products, the fragmentation patterns are approximately the same with each other and with simple SCNT. However, some irregularities have been observed in 300–700 °C region that might be due to the interaction or reaction of GNPs with the fragmented species. As a result, gold decoration did not change the thermal stability of SCNTs meaningfully and there is no remarkable difference between the thermal stabilities of decorated products with different gold content.

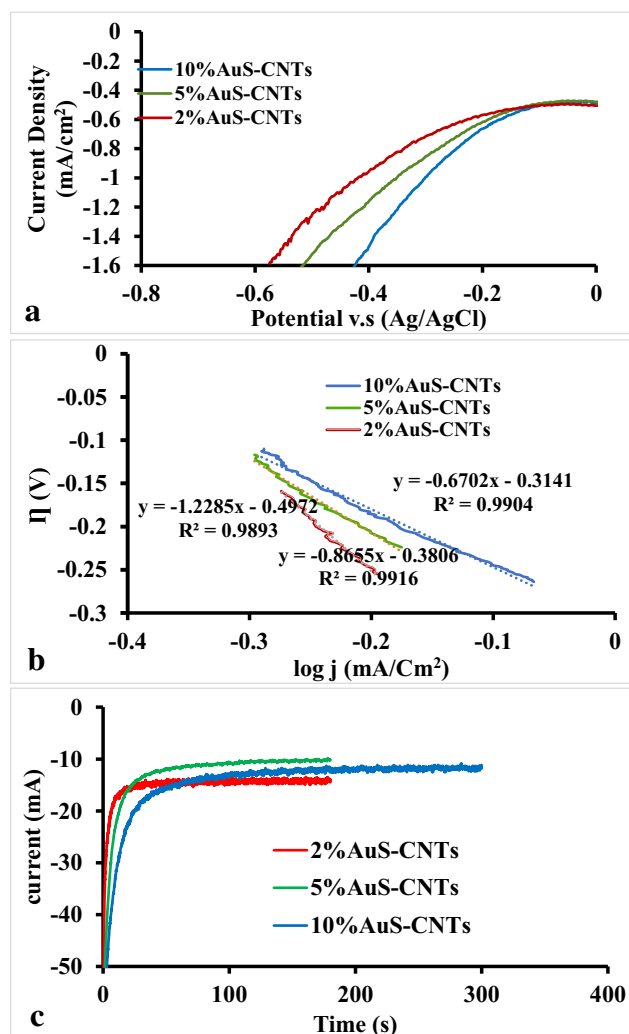


Fig. 12 a The LSV curves of the Au-SCNTs in alkaline HER (in 1 M KOH). b The Tafel slope charts for Au-SCNTs as HER electrocatalyst. c The chronoamperometric diagrams for Au-SCNTs

The electrochemical behaviors of the products

As a useful application for the prepared products, both undecorated SCNTs and three decorated ones have been employed as an electrocatalyst in HER. Linear sweep voltammetry (LSV) experiments were performed to obtain the overpotential for SCNTs grown over Co/SiO₂ (SCNTs-Co/SiO₂) and Co⁰ (SCNTs-Co). Moreover, the same experiments were performed on the three decorated products, and the brief results are gathered in Table 2. The LSV diagrams and Tafel slope charts for SCNTs are depicted in Fig. 11. According to these values, SCNTs-Co/SiO₂ with −1.3 V initial overpotential and 255 mV dec^{−1} Tafel slope has better functionality and stability in comparison with SCNTs-Co which shows −2.65 V overpotential and 565 mV dec^{−1} Tafel slope. The lower the initial overpotential for reaction initiation, the lower the energy required for water splitting which makes the HER more energy-efficient. Additionally, the lower the Tafel

slope, the faster the kinetics of the reaction and the higher the electrocatalytic activity. Therefore, in addition to the more appropriate morphology and basic characteristics of SCNTs-Co/SiO₂ versus SCNTs-Co, its lower initial overpotential and Tafel slope make it better candidate and more effective electrocatalyst in HER.

Since SCNTs-Co/SiO₂ shows the more reliable results than SCNTs-Co, this sample has been chosen for further electrochemical investigations. According to the previously mentioned method (“The preparation of catalysts” section), various amounts of GNPs (2, 5, and 10%) were decorated on the surface of this sample to prepare three decorated products. The LSV data from application of gold decorated sulfur doped carbon nanotubes (Au-S-CNTs) are also shown in Table 2. Moreover, the corresponding LSV diagrams, Tafel slope plots, and chronoamperometric curves for these products are depicted in Fig. 12. Among all decorated products, 10% Au-SCNTs showed the best ability with -0.496 V initial overpotential and 670 mV dec⁻¹ Tafel slope in comparison with 5% Au-SCNTs with -0.498 V overpotential and 850 mV dec⁻¹ Tafel slope and 2% Au-SCNTs with -0.495 V overpotential and 1228 mV dec⁻¹ Tafel slope. The initial overpotential of these catalysts is nearly the same, and their difference is related to the Tafel slopes.

Finally, chronoamperometry experiments were used to assess the electrochemical stability of various Au-SCNTs. This diagram shows the time dependence of current density under static potential versus RHE. The current density remains no degradation after 190 s, which further demonstrate the stability of Au-SCNTs. The excellent stability and strong durability of 10% Au-SCNTs is mainly attributed to the excellent decoration of GNPs on SCNT surface. The outstanding electrocatalytic activity as well as stability of the Au-SCNT catalysts may make them a promising HER catalyst for practical applications.

Conclusion

In summary, to prepare the desired SCNTs, different cobalt catalysts, four different temperatures (600, 650, 700, and 750 °C), and various growth parameters have been employed. Among the employed condition, Co/SiO₂ catalyst (and then Co catalyst) at 600 °C was selected as the best conditions. The electrochemical behaviors of the two best products (SCNTs-Co/SiO₂ and SCNTs-Co) in HER were examined, which the product prepared on Co/SiO₂ catalyst showed higher abilities. Then, the best product was decorated with 2, 5, and 10% of GNPs to examine the effect of gold decoration of the properties and electrochemical abilities of the product. After the complete analysis of the decorated products, which showed similar or better properties than simple ones, they have been employed in HER. The results showed higher abilities of

decorated products versus simple SCNTs, and all of them showed high stabilities and appropriate electrocatalytic behaviors in HER, especially 10% Au-SCNT products.

References

- Jang JU, Cha JE, Lee SH, Kim J, Yang B, Kim SY, Kim SH (2019) Enhanced electrical and electromagnetic interference shielding properties of uniformly dispersed carbon nanotubes filled composite films via solvent-free process using ring-opening polymerization of cyclic butylene terephthalate. *Polymer*, 122030
- Hung NT, Nugraha AR, Saito R (2019) Thermoelectric properties of carbon nanotubes. *Energies* 12(23):4561
- Dai K, Hu T, Zhang J, Lu L (2019) Carbon nanotube exfoliated porous reduced graphene oxide/CdS-diethylenetriamine heterojunction for efficient photocatalytic H₂ production. *Appl Surf Sci*, 144783
- Vijayabhaskar A, Shanmugasundaram M (2017) Usage of carbon nanotubes and nanofibers in cement and concrete: a review. *Int J Eng Technol* 9:564–569
- Scarselli M et al (2015) Applications of three-dimensional carbon nanotube networks. *Beilstein J Nanotechnol* 6:792–798
- Thines RK, Mubarak NM, Nizamuddin S, Sahu JN, Abdullah EC, Ganesan P (2017) Application potential of carbon nanomaterials in water and wastewater treatment: a review. *J Taiwan Inst Chem Eng* 72:116–133
- Brady-Estévez AS, Nguyen TH, Gutierrez L, Elimelech M (2010) Impact of solution chemistry on viral removal by a single-walled carbon nanotube filter. *Water Res* 44:3773–3780
- Hashim DP et al (2012) Covalently bonded three-dimensional carbon nanotube solids via boron induced nanojunctions. *Sci Rep* 2:1–8
- Licht S, Douglas A, Ren J, Carter R, Lefler M, Pint CL (2016) Carbon nanotubes produced from ambient carbon dioxide for environmentally sustainable lithium-ion and sodium-ion battery anodes. *ACS Cent Sci* 2:162–168
- Alimohammadi F, Gashti MP, Shamei A (2012) A novel method for coating of carbon nanotube on cellulose fiber using 1,2,3,4-butanetetracarboxylic acid as a cross-linking agent. *Prog Org Coat* 74:470–478
- Alimohammadi F, Parvinzadeh Gashti M, Shamei A (2013) Functional cellulose fibers via polycarboxylic acid/carbon nanotube composite coating. *J Coat Technol Res* 10:123–132
- Coleman JN, Khan U, Blau WJ, Gun'ko YK (1624–1652) Small but strong: a review of the mechanical properties of carbon nanotube-polymer composites. *Carbon* 44:2006
- Chen P, Kim HS, Kwon SM, Yun YS, Jin HJ (2009) Regenerated bacterial cellulose/multi-walled carbon nanotubes composite fibers prepared by wet-spinning. *Curr Appl Phys* 9:96–99
- Gabor NM, Zhong Z, Bosnick K, Park J, McEuen PL (2009) Extremely efficient multiple electron-hole pair generation in carbon nanotube photodiodes. *Science* 5946:1367–1371
- Benthall J (2012) Believing in belonging: belief and social identity in the modern world. *J R Anthropol Inst* 18:495–496
- Li WS, Chang ML, Cheng HC (2019) Facile synthesis of CNTs/Co(OH) 2 hybrid nanostructures for high-performance electrochemical supercapacitor. *Chem Phys Lett*, 137003
- Lee JM, Park JS, Lee SH, Kim H, Yoo S, Kim SO (2011) Selective electron- or hole-transport enhancement in bulk-heterojunction organic solar cells with N- or B-doped carbon nanotubes. *Adv Mater* 23:629–633

18. Sakamoto JS, Dunn B (2002) Vanadium oxide-carbon nanotube composite electrodes for use in secondary lithium batteries. *J Electrochem Soc* 149:A26
19. Veedu VP, Cao A, Li X, Ma K, Soldano C, Kar S, Ajayan PM, Ghasemi-Nejhad MN (2006) Multifunctional composites using reinforced laminae with carbon-nanotube forests. *Nat Mater* 5:457–462
20. Le Goff A et al (2009) From hydrogenases to noble metal-free catalytic nanomaterials for H₂ production and uptake. *Science* 325:1384–1387
21. Bianco A, Kostarelos K, Prato M (2005) Applications of carbon nanotubes in drug delivery. *Curr Opin Chem Biol* 9:674–679
22. Kam NWS, Jessop TC, Wender PA, Dai H (2004) Nanotube molecular transporters: internalization of carbon nanotube-protein conjugates into mammalian cells. *J Am Chem Soc* 126:6850–6851
23. Cai D, Mataraza JM, Qin ZH, Huang Z, Huang J, Chiles TC, Carnahan D, Kempa K, Ren Z (2005) Highly efficient molecular delivery into mammalian cells using carbon nanotube spearing. *Nat Methods* 2:449–454
24. Huang H, Yu Y, Zhang M (2019) Analysis of adsorption properties of SF₆ decomposed gases (SOF₂, SO₂F₂, SF₄, CF₄, and HF) on Fe-doped SWCNT: a DFT study. *Appl Surf Sci*, 144622
25. Terrava ML, Sessa V, Rossi M (2006) The world of carbon nanotubes: an overview of CVD growth methodologies. *Chem Vap Depos* 12:315–325
26. José-Yacamán M, Miki-Yoshida M, Rendón L, Santiesteban JG (1993) Catalytic growth of carbon microtubules with fullerene structure. *Appl Phys Lett* 62:202–204
27. Chiang M-R, Liu K-S, Lai T-S, Tsai C-H, Cheng H-F, Lin I-N (2001) Electron field emission properties of pulsed laser deposited carbon films containing carbon nanotubes. *J Vac Sci Technol B* 19: 1034
28. Ajayan PM (1787–1800) Natubes from carbon. *Chem Rev* 99:1999
29. Choi E, Gao Y, Cui Y, Pyo SG (2019) Effects of Ti-based interposer layer on graphene/carbon nanotube nano-contact resistance. *Appl Surf Sci*, 144881
30. Chen J et al (1998) Solution properties of single-walled carbon nanotubes. *Science* 281:95–98
31. Yang Q, Xu W, Tomita A, Kyotani T (2005) Double coaxial structure and dual physicochemical properties of carbon nanotubes composed of stacked nitrogen-doped and undoped multiwalls. *Chem Mater* 17:2940–2945
32. Nxumalo EN, Coville NJ (2010) Nitrogen doped carbon nanotubes from organometallic compounds: a review. *Materials (Basel)* 3:2141–2171
33. Hamadani M, Khoshnevisan B, Fotooh FK (2011) Density functional study of super cell N-doped (10,0) zigzag single-walled carbon nanotubes as CO sensor. *Struct Chem* 22:1205–1211
34. Zhang X, Gong X (2015) Theoretical investigation of rare gas adsorption on and inside B-doped carbon nanotubes by DFT, QTAIM and NBO. *RSC Adv* 5:65604–65612
35. Hassani F, Tavakol H, Keshavarzipour F, Javaheri A (2016) A simple synthesis of sulfur-doped graphene using sulfur powder by chemical vapor deposition. *RSC Adv* 6:27158–27163
36. Maukian M, Tavakol H, Fashandi H (2018) Synthesis of highly uniform sulfur-doped carbon sphere using CVD method and its application for cationic dye removal in comparison with undoped product. *J Environ Chem Eng* 6:6904–6915
37. Bakhshi P, Tavakol H (2019) Synthesis of Si-doped CNT and its catalytic ability in hydrogen evolution reaction, 1–7
38. Masatake H (2004) Gold as a novel catalyst in the 21st century: preparation, working mechanism and applications. *Gold Bull* 37: 27–36
39. Geoffrey B, Thompson DT (2000) Gold-catalysed oxidation of carbon monoxide. *Gold Bull* 33:41–50
40. Hashmi ASK (2003) Homogeneous gold catalysts and alkynes: a successful liaison. *Gold Bull* 36:3–9
41. Hashmi ASK, Hutchings GJ (2006) Gold catalysis. *Angew Chem Int Ed* 45:7896–7936
42. Zheng Y, Jiao Y, Vasileff A, Qiao SZ (2018) The hydrogen evolution reaction in alkaline solution: from theory, single crystal models, to practical electrocatalysts. *Angew Chem Int Ed* 57:7568–7579
43. Zhou W et al (2016) Recent developments of carbon-based electrocatalysts for hydrogen evolution reaction. *Nano Energy* 28: 29–43
44. Ponder SM, Darab JG, Mallouk TE (2000) Remediation of Cr(VI) and Pb(II) aqueous solutions using supported, nanoscale zero-valent iron. *Environ Sci Technol* 34:2564–2569
45. Bhavani P, Reddy NR, Reddy IVS (2017) Synthesis and physical characterization of γ -Fe₂O₃ and (α + γ)-Fe₂O₃ nanoparticles. *J Korean Phys Soc* 70:150–154
46. Martin MN, Basham JI, Chando P, Eah S (2010) Charged gold nanoparticles in non-polar solvents: 10-min synthesis and 2D self-assembly, 26, 7410–7417
47. Yagi T, Marumo F, Akimoto SI (1974) Crystal structures of spinel polymorphs of Fe₂SiO₄ and Ni₂SiO₄. *Am Mineral* 59:486–490
48. Saib AM, Borgna A, van de Loosdrecht J, van Berge PJ, Geus JW, Niemantsverdriet JW (2006) Preparation and characterisation of spherical Co/SiO₂ model catalysts with well-defined nano-sized cobalt crystallites and a comparison of their stability against oxidation with water. *J Catal* 239:326–339
49. Uosaki K, Shen Y, Kondo T (2000) Preparation of a highly ordered Au (111) phase on a polycrystalline gold substrate by vacuum deposition and its characterization by XRD, GISXRD, STWAFM, and electrochemical measurements, 111, 14117–14122

Publisher's note Springer Nature remains neutral with regard to jurisdictional claims in published maps and institutional affiliations.